



## Subpolar gyre decadal variability explains the recent oxygenation in the Irminger Sea

Charlène Feucher, Esther Portela, Nicolas Kolodziejczyk, Virginie Thierry

### ► To cite this version:

Charlène Feucher, Esther Portela, Nicolas Kolodziejczyk, Virginie Thierry. Subpolar gyre decadal variability explains the recent oxygenation in the Irminger Sea. *Communications Earth & Environment*, 2022, 3 (1), 279 (9p.). 10.1038/s43247-022-00570-y . hal-04203923

**HAL Id: hal-04203923**

**<https://hal.science/hal-04203923>**

Submitted on 15 Sep 2023

**HAL** is a multi-disciplinary open access archive for the deposit and dissemination of scientific research documents, whether they are published or not. The documents may come from teaching and research institutions in France or abroad, or from public or private research centers.

L'archive ouverte pluridisciplinaire **HAL**, est destinée au dépôt et à la diffusion de documents scientifiques de niveau recherche, publiés ou non, émanant des établissements d'enseignement et de recherche français ou étrangers, des laboratoires publics ou privés.



Distributed under a Creative Commons Attribution 4.0 International License

## Subpolar gyre decadal variability explains the recent oxygenation in the Irminger Sea

Charlène Feucher<sup>1</sup>  , Esther Portela<sup>1,2</sup>, Nicolas Kolodziejczyk<sup>1</sup>  & Virginie Thierry<sup>1</sup> 

Accurate monitoring of the long-term trend of oxygen content at global scale requires a better knowledge of the regional oxygen variability at interannual to decadal time scale. Here, we combined the Argo dataset and repeated ship-based sections to investigate the drivers of the oxygen variability in the North Atlantic Ocean, a key region for the oxygen supply into the deep ocean. We focus on the Labrador Sea Water in the Irminger Sea over the period 1991–2018 and we show that the oxygen solubility explains less than a third of the oxygen variability. In turn, the main drivers of the oxygen variability are due to changes in vertical mixing, advection, and other processes as revealed by Apparent Oxygen Utilization computation. Our findings revealed the key role of physical processes on the changes in oxygen variability and highlight the need of keeping a sustained monitoring of those processes to disentangle human-induced changes in oxygen from decadal natural variability.

<sup>1</sup> Univ Brest, CNRS, Ifremer, IRD, LOPS, Plouzané F-29280, France. <sup>2</sup> Institute for Marine and Antarctic Studies, University of Tasmania, Hobart 7001, Australia.  
✉email: [charlene.feucher@gmail.com](mailto:charlene.feucher@gmail.com)

Over the last 50 years, the global ocean has lost around 2% of the dissolved oxygen inventory<sup>1</sup>. Climate-model projections predict that the current deoxygenation trend will continue<sup>1,2</sup>, and even intensify over the next century<sup>3</sup>. The observed global-ocean deoxygenation trend over the past decades has been attributed to a combination of a warming-induced decline in oxygen due to a lower solubility<sup>1</sup> (25% in the first 1000 m depth), and reduced ocean ventilation due to increased upper ocean stratification<sup>1,4,5</sup>. However, the uncertainties of those projections are still important because the regional and interannual-to-decadal variability of the ocean oxygen content are poorly documented<sup>4,6</sup>. This is particularly true in the main ventilation areas of subtropical and subpolar latitudes, which play a crucial role for the oxygen supply into the ocean interior, and for the present and the future ocean deoxygenation<sup>7,8</sup>.

In the North Atlantic Ocean (Fig. 1), the Labrador and Irminger seas are recognized as important regions for ocean ventilation and oxygen uptake<sup>9–11</sup>. There, the massive mixing between mixed-layer waters, nearly saturated in oxygen, and undersaturated subsurface waters take place during winter deep convection<sup>12,13</sup>. This process is responsible for the formation of the weakly stratified Labrador Sea Water (LSW), which conveys oxygenated waters into the deep ocean. Then, ocean circulation transports those oxygen-rich waters away from their sources across the entire Atlantic Basin<sup>14</sup>. For instance, in deep convection regions as the Irminger Sea, the oxygen concentration within the mixed layer is close to saturation<sup>12,13,15,16</sup> (i.e. around 93%). Local mixing and consumption, as well as remote oxygen advection, can also modulate the local oxygen concentration, but the role of these mechanisms in setting the oxygen content in the Irminger Sea remains unclear.

In this context, the Irminger basin is of special interest since recent observations have suggested a return of deep convection there in the last years, with a potential impact on oxygen

ventilation<sup>11,15,17,18</sup>. For instance, stronger convection was attributed to stronger westerly winds and intense heat loss from the ocean during the positive North Atlantic Oscillation (NAO) phase<sup>19</sup>. At interannual scale, the occurrence of intense wind stress events, the Greenland tip jets, also favors deep convection in the Irminger Sea<sup>15</sup>. In some of these studies, oxygen concentration has been used to investigate deep convection and ventilation processes at seasonal to interannual scales<sup>11,13,15,18,20–22</sup>. At decadal scale, the subpolar gyre is also subjected to strong variability. Cooling and freshening (warming and salinification) of the subpolar gyre has been associated with a gyre strengthening<sup>23</sup> (weakening). Cold and fresh conditions also play a role in the preconditioning of the water column for deep convection events through changes in circulation and stratification<sup>18,24</sup>.

In this study, we investigate the decadal variability of the dissolved oxygen of the LSW in the Irminger Sea and its driving processes over the period 1991–2018. The most updated Argo dataset, combined with the available hydrographic sections, provide us with a unique time series of physical variables and oxygen concentration to address this question. Particularly, we focus on: (i) describing the change in oxygen concentration in the Irminger Sea over the last three decades, and (ii) attributing the observed oxygen variability within the LSW layer in the Irminger Sea to the driving physical processes.

The article is organized as follows: “Results” section describes the variability of the dissolved oxygen concentration in the Irminger Sea with a focus on the LSW. Results are then discussed and conclusions drawn in the section “Discussion and conclusion”. “Methods” section describes the datasets and methods used in this study.

## Results

Over the whole sampling period, the LSW density varies between 27.7 and 27.8 kg m<sup>−3</sup> (Fig. 2), and its mean properties are  $\theta = 3.5 \pm 0.1$  °C,  $S = 34.88 \pm 0.02$ , and oxygen concentration of  $292.9 \pm 2.1$   $\mu\text{mol kg}^{-1}$  (Figs. 3 and 4). However, LSW properties exhibit strong interannual to decadal variability that allows to roughly distinguish three different periods: P1: 1991–1997, P2: 2002–2014, and P3: 2015–2018. These three periods are highlighted as in Fig. 2.

Between 1991 and 1997 (P<sub>1</sub>), the LSW is relatively cold ( $3.2 \pm 0.02$  °C), fresh (34.86), and dense ( $\sigma_\theta \approx 27.77$  kg m<sup>−3</sup>). The weak stratification during this period results in a thick LSW layer (around 870 m) that extends down to 1500 m (Fig. 3). This thick LSW is characterized by high oxygen concentration ( $297.8 \pm 3.10$   $\mu\text{mol kg}^{-1}$ ), and low apparent oxygen utilization (AOU;  $25 \pm 3$   $\mu\text{mol kg}^{-1}$ ) (Figs. 2b, c and 3b). During this period, the hydrographic properties and oxygen concentration showed little variability with no changes in AOU and oxygen at saturation  $\text{O}_2^{\text{sat}}$ .

Over the period 2002–2014 (P<sub>2</sub>), the LSW was, on average, warmer ( $3.8 \pm 0.22$  °C), saltier ( $34.90 \pm 0.01$ ), and lighter ( $27.74 \pm 0.02$  kg m<sup>−3</sup>) than during the previous period. The LSW layer was also thinner, more stratified (thickness < 500 m), and shallower, with maximum depth around 1000 m (Figs. 3 and 4). These changes in LSW properties are accompanied by a decrease in the oxygen concentration as compared to the previous P<sub>1</sub> period ( $287.2 \pm 3.8$   $\mu\text{mol kg}^{-1}$ ). During the first half of P<sub>2</sub> (between 2002 and 2008), we observe a progressive decrease of both,  $\text{O}_2^{\text{sat}}$  and AOU, while the oxygen concentration slightly increases (Fig. 2). AOU increases again during the second half of P<sub>2</sub> (2010–2014) while  $\text{O}_2^{\text{sat}}$  remains low and nearly constant.

Finally, from 2015 to 2018 (P<sub>3</sub>), the Argo data reveal an abrupt increase of oxygen concentration in the LSW of about 15  $\mu\text{mol kg}^{-1}$  (from <280  $\mu\text{mol kg}^{-1}$  in 2015 to around

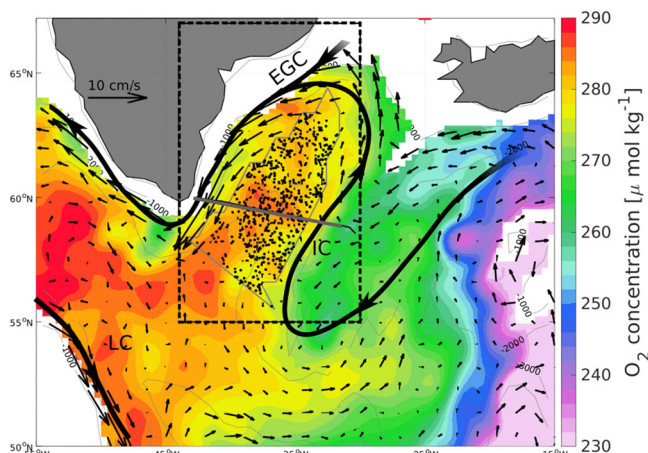


**Fig. 1 Oxygen concentration and main circulation in the North Atlantic Ocean.** Mean oxygen concentration averaged between 900 and 1100 m depth as computed from ISAS (color-coded). The location of the Argo profiles used in this study is represented by black dots within the bathymetric contour of 2700 m that we used to define the core of the Irminger Sea (gray contour). The gray line shows the average location of the hydrographic sections (OVIDE, AR07E, A01E). The black, thick curve represents the surface current, and the main currents in the region, i.e. the Eastern Greenland current (EGC), the Irminger Current (IC) and the Labrador Current (LC), and it is superimposed to the mean circulation at 1000 m (computed from ANDRO). The dashed rectangle represents the region where we average the Wind Stress Curl (WSC), the relative vorticity on the ocean circulation at 1000 m and the detrended annual-mean Sea Level Anomaly (SLA) (Fig. 5).

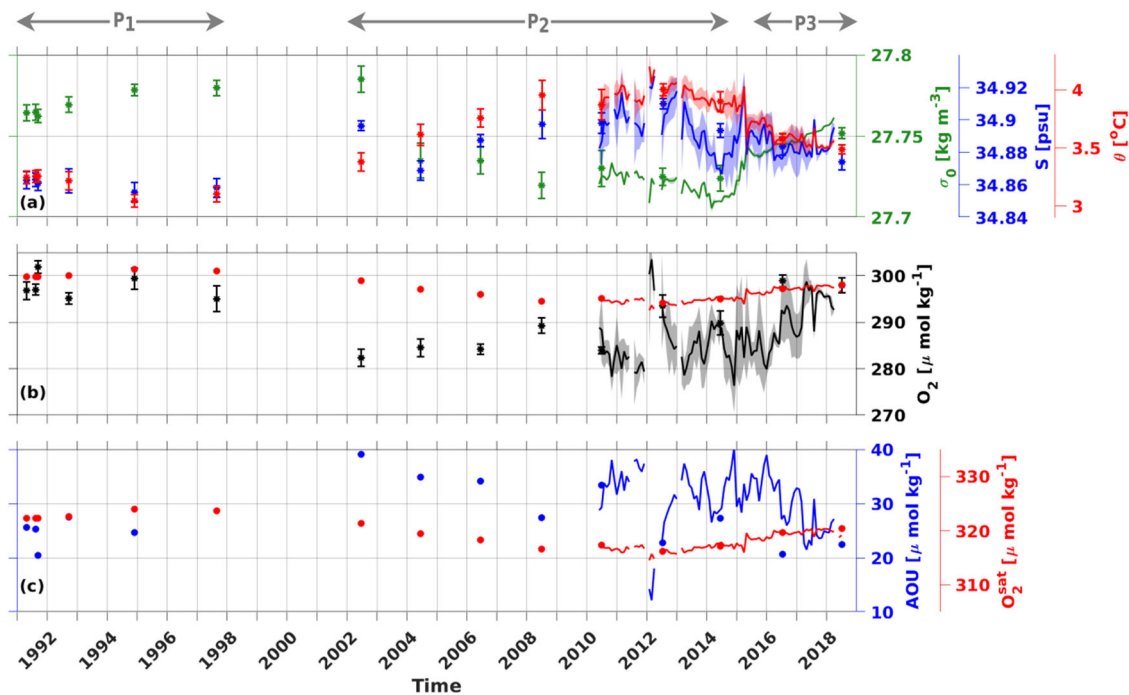


**Fig. 2 Temporal variability of the Labrador Sea Water properties in the Irminger Sea.** **a** Salinity (blue curve; psu), potential temperature  $\theta$  (red curve; °C), and potential density  $\sigma_0$  (green curve;  $\text{kg m}^{-3}$ ). **b** Oxygen concentration  $\text{O}_2$  (black curve;  $\mu\text{mol kg}^{-1}$ ) and the oxygen at 93% of saturation (red curve and dots). **c** Apparent Oxygen Utilization AOU (blue curve;  $\mu\text{mol kg}^{-1}$ ) and oxygen at saturation  $\text{O}_2^{\text{sat}}$  (red curve;  $\mu\text{mol kg}^{-1}$ ). Plain curves represent Argo data, and dots represent the hydrographic sections. The uncertainty for the Argo data is computed as the standard deviation around the spatial average (gray shading), and for the hydrographic section it is computed as the standard deviation over the layer depth (error bars). The three periods ( $P_1$ ,  $P_2$ , and  $P_3$ ) discussed throughout the manuscript are indicated with arrows on top of the figure.

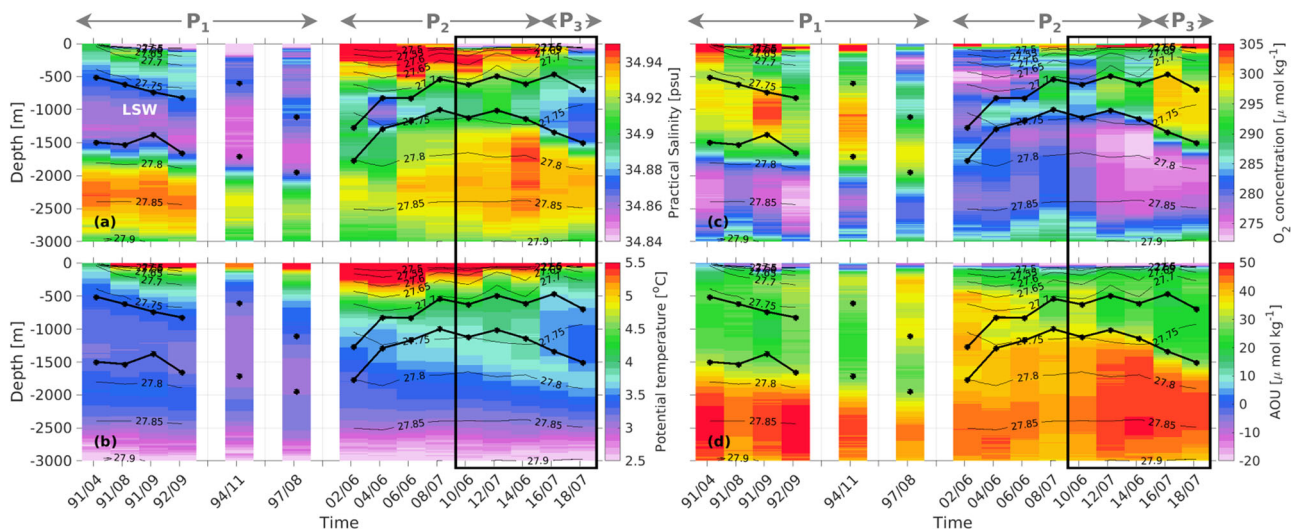


**Fig. 3 Temporal variability of the water properties in the Irminger Sea from hydrographic sections.** Variability between 1991 and 2018 of **a** practical salinity (psu), **b** potential temperature  $\theta$  (°C), **c** oxygen concentration ( $\mu\text{mol kg}^{-1}$ ), and **d** Apparent Oxygen Utilization AOU ( $\mu\text{mol kg}^{-1}$ ) computed along the hydrographic sections (OVIDE, A01E, AR07E) within the Irminger Sea (longitudes between 40° W and 35° W). The black square denotes the period covered by Argo sampling as shown in Fig. 3, and the black solid lines with dots highlight the upper and lower boundaries of the Labrador Sea Water (LSW) layer. Note that the x-axis is not evenly spaced, and that the longest gaps are marked with a blank space. The three periods ( $P_1$ ,  $P_2$ , and  $P_3$ ) discussed throughout the manuscript are indicated with arrows on top of the figure.

$295 \mu\text{mol kg}^{-1}$  in 2018, Figs. 2 and 4). The latter is accompanied by a dramatic shallowing of the  $27.75 \text{ kg m}^{-3}$  isopycnal of  $\approx 800 \text{ m}$  from 2016 to 2018 (Fig. 2). The LSW layer was slightly thinner (700 m) and shallower (maximum depth  $\approx 1300 \text{ m}$ ) than in the 90's (Fig. 3). During  $P_3$ , the upper stratification in the Irminger Sea diminished in comparison with the previous  $P_2$  period, which is consistent with the observed increase of the LSW thickness

(Figs. 2 and 4). The strong oxygenation of the LSW ( $289.6 \pm 5.3 \mu\text{mol kg}^{-1}$ ) is accompanied by a recovering of cold ( $3.6 \pm 0.1^\circ\text{C}$ ), fresh ( $34.9$ ) and dense ( $27.75 \pm 0.01 \text{ kg m}^{-3}$ ) properties comparable to those of the 90's ( $P_1$ ) (Fig. 3). Over the whole 1991–2018 period, the variance of the LSW oxygen concentration was  $41.8 \mu\text{mol}^2 \text{ kg}^{-2}$ , while that of the oxygen solubility and AOU were  $7.0 \mu\text{mol}^2 \text{ kg}^{-2}$  and  $30.6 \mu\text{mol}^2 \text{ kg}^{-2}$ ,



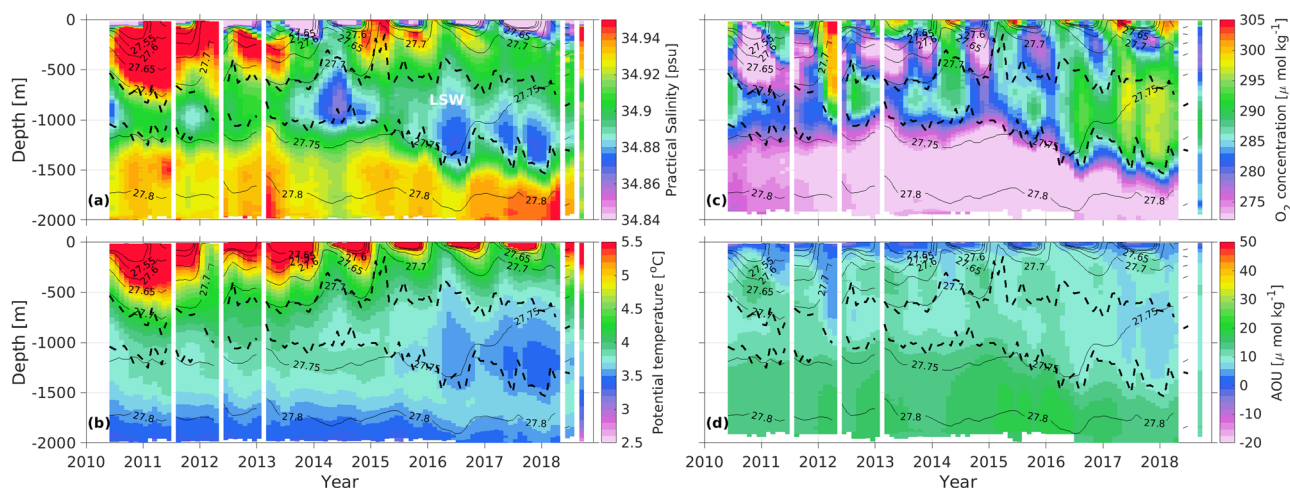


**Fig. 4 Temporal variability of the water properties in the Irminger Sea from Argo data.** Variability between 2010 and 2018 of **a** salinity (psu), **b** potential temperature  $\theta$  (°C), **c** oxygen concentration ( $\mu\text{mol kg}^{-1}$ ), and **d** Apparent Oxygen Utilization AOU ( $\mu\text{mol kg}^{-1}$ ) computed from Argo data in the Irminger Sea. The dashed black contours highlight the lower and upper boundaries of the Labrador Sea Water (LSW) layer. Note that the vertical white lines indicate missing data for interpolation.

respectively. Changes in solubility ( $\text{O}_2^{\text{sat}}$ ) account for only about 17% of the total oxygen variability and cannot explain most of the decadal variability of the oxygen concentration in the LSW. In contrast, processes related to AOU changes account for about 73% of the  $\text{O}_2$  variability (Fig. 2c). This reveals that mixing, advection and consumption are important drivers of the observed oxygen variability.

During 1991–1997 ( $P_1$ ) and 2017–2018 (last years of  $P_3$ ), the oxygen concentration of the LSW is close to the 93% of  $\text{O}_2^{\text{sat}}$ , i.e. the typical saturation of fairly recently ventilated LSW (Fig. 2b). Over these periods, the estimated AOU is relatively low, and can mainly be attributed to convective mixing between young, oxygen-rich waters in the mixed layer, and less oxygenated waters below. In contrast, during the 2002–2014 period ( $P_2$ ), as well as in 2015–2016 (first years of  $P_3$ ), the observed oxygen concentration is lower than the 93% of  $\text{O}_2^{\text{sat}}$ . Interestingly both, the solubility and AOU, diminish during the  $P_2$  period, which exhibits important variability. LSW is oldest at the beginning of the period while the LSW starts to get warmer. During  $P_2$ , the decrease in AOU also coincides with a strong decrease in the LSW core density, from 27.78 in 2002 to 27.73 after 2004. Part of this might be due to the presence of two different types of LSW, i.e., the 1987–1994 LSW and the 2000–2003 LSW with the former being much older<sup>10</sup>. During this period, given the weak convection in the Irminger Sea, the presence of older water could be explained by a combination of an advection of LSW from the Labrador Sea and a slow drainage of the available LSW volume, rather than by local ventilation through winter convection. However, from 2002 to 2014 ( $P_2$ ), the interannual variability in the oxygen concentration of LSW as well as in its age (AOU) can be partly explained by convective events visible in 2008, 2009, and 2012 (Figs. 2 and 4) and reported in previous studies<sup>11,15,18,21,25</sup>.

As suggested by the important variability of the AOU over the sampling record, changes in the oxygen concentration of the LSW are strongly related to mixing and advection processes. The contribution of biological respiration, also possible although unlikely to have a major role in this region, is beyond the scope of the present study. Therefore, we investigated the temporal variability of three processes that could contribute to the observed changes in the oxygen concentration of the LSW: (i) the convection depth (given by the MLD), that accounts for the direct ventilation of the LSW during the boreal winter; (ii) the wind stress curl, that spins up/down the subpolar gyre, and influences

temperature, salinity, stratification and advection<sup>26</sup> (Fig. 5), and (iii) the mixed layer temperature that controls oxygen solubility. All three processes are linked to the NAO index (i.e. positive/negative NAO anomalies, Fig. 5a).

We first investigated the link between the changes in oxygen concentration and the change in the circulation at 1000 m depth (approximately the mean depth of the LSW) within the extended region of the Irminger Sea (see the dashed black rectangle in Fig. 1). We used the anomaly of the relative vorticity of the velocity field at 1000 m depth as a proxy of the intensity of the gyre (Fig. 5c, horizontal black lines). From 2002 to 2014 ( $P_2$ ), when oxygen concentration was low in the LSW, we observed that the circulation of the subpolar gyre at 1000 m depth is weaker. Then, during the transition to the periods of high oxygen concentration ( $P_2$  to  $P_3$ ), the circulation has intensified in about  $1.2 \times 10^{-7} \text{ s}^{-1}$ . Since we do not have Argo data available in  $P_1$ , we complemented the gyre intensity by an other proxy: the Sea Level Anomaly (SLA). The variability of the SLA is consistently anticorrelated with the anomaly of the relative vorticity at 1000 m, suggesting a mostly barotropic gyre circulation. Between 2002 and 2014 ( $P_2$ ) when the gyre is less intense, the SLA is positive, and the opposite occurs during the period 2015–2018 ( $P_3$ ). Despite satellite data are only available from 1993, the SLA anomaly suggests that the slowdown of the subpolar gyre is likely to occur during the second half of the 90s, when the SLA anomaly transitions from negative to positive. The intensity of the subpolar gyre near 1000 m depth is in general agreement with the enhancement of the winter Wind Stress Curl (WSC) in the Irminger Sea (Fig. 5a). We observe that the strength of the gyre is significantly anti-correlated (at 95% confidence level), with a 2 year-lag, with the annual WSC ( $r = -0.5$ , WSC leading). During  $P_1$  and  $P_3$ , the NAO and WSC anomalies are mainly positive, with respective maxima in 2015 (Fig. 5a), while there were negative between 2002 and 2014 ( $P_2$ ). This is associated with a change in the hydrographic properties and stratification of the upper water column: during  $P_1$  and  $P_3$  ( $P_2$ ), the upper layer is cold (warm) and the stratification is low (high), and the oxygen concentration in the LSW is high (low).

The variability of the circulation of the subpolar gyre as well as the WSC are also well correlated with the temperature and depth of the mixed layer (i.e. convection depth, (Fig. 5b)). During the period 2015–2017 the Mixed Layer Depth (MLD) reached its maximum depth (between 1000 and 2000 m) and minimum

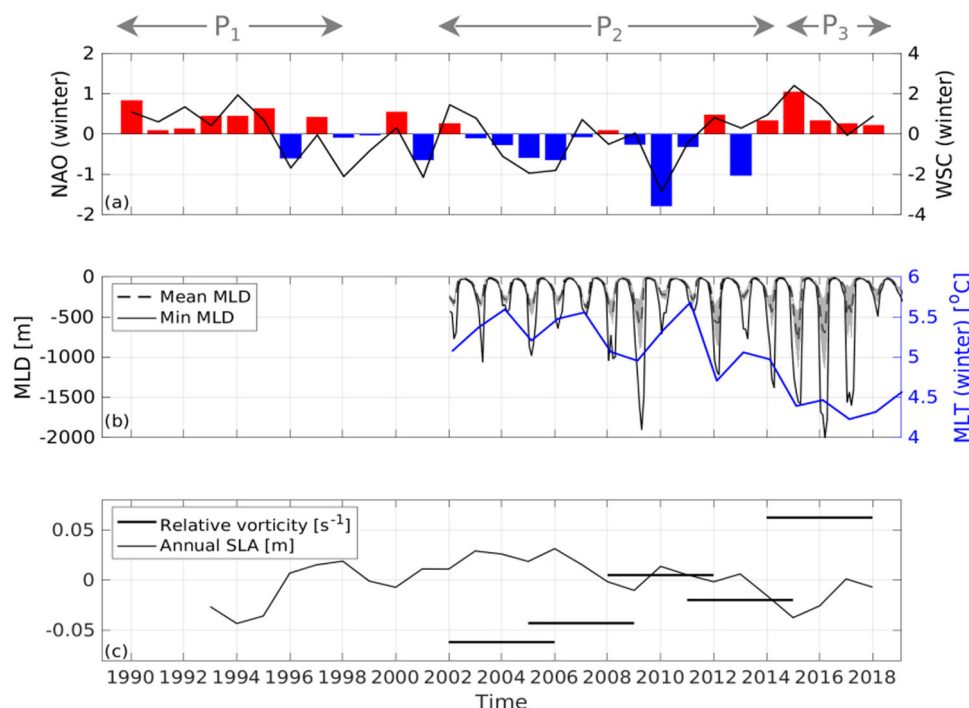


**Fig. 5 Temporal variability of the North Atlantic subpolar gyre properties.** **a** Winter North Atlantic Oscillation (NAO) index anomalies from 1990 to 2018, and winter Wind Stress Curl (WSC;  $\text{N m}^{-2}$ ) from 1990 to 2018 (black curve) in the Irminger Sea. **b** Monthly Mixed Layer Depth (MLD; black curve) and Mixed Layer Temperature (MLT;  $^{\circ}\text{C}$ , blue curve) averaged in the Irminger Sea region from 2002 to 2018 computed from ISAS. The uncertainty in the mean MLD is computed as one standard deviation around the mean value. **c** The black curve represents the annual Sea Level Anomalies (SLA), detrended and offset by its mean (2.7 cm). The horizontal lines show the anomaly of the relative vorticity at 1000 m and average over 4-years periods. The three periods ( $P_1$ ,  $P_2$ , and  $P_3$ ) discussed throughout the manuscript are indicated with arrows on top of the figure.

temperature ( $\text{MLT} < 4.5^{\circ}\text{C}$ )), which evidences the occurrence of strong winter convection in the Irminger Sea (Fig. 5b). During this period, the winter MLD is deep enough to reach and ventilate the LSW layer and increase the local injection of oxygen (Fig. 2). In turn, in 2018, the last year of  $P_3$ , we observe a weak convection and warmer mixed layer, which is in agreement with weak North Atlantic Oscillation (NAO), SLA and WSC anomalies. Shallower and warmer MLD associated to negative NAO and WSC anomalies were also observed during the 2002–2014 period. This shift in the atmospheric forcing during  $P_2$  is in agreement with the slowdown of the subpolar gyre in the Irminger basin (Fig. 5c), with the presence of a warmer and more stratified surface layer, and with shallower convection.

Due to the lack of Argo data before 2002, we cannot compute the seasonal mixed layer depth and properties before this year. However, the variability of the NAO can be linked to the observed characteristics of the LSW in the 90s. As during the 2015–2018 and 1990–1997 periods, the NAO and WSC anomalies are positive and relatively strong.

## Discussion and conclusion

In this study, an oxygen dataset covering almost three decades between 1991 and 2018 has revealed strong interannual to decadal variability in the oxygen concentration within the LSW layer. High oxygen concentration ( $\approx 300 \mu\text{mol kg}^{-1}$ ) is observed in the LSW between 1991 and 1997 ( $P_1$ ). After a 5-year data gap, from 2002 to 2014 ( $P_2$ ), LSW became lighter, warmer and less oxygenated ( $\approx 280 \mu\text{mol kg}^{-1}$ ), but from 2015 to 2018 ( $P_3$ ) the characteristics of LSW recovered to those observed in the 90s decade. Interestingly, the available record appears to resolve one cycle of the subpolar gyre in Irminger Sea in which the oxygen and hydrographic conditions of the 90s are mostly recovered at the end of the period.

The analyses carried out here shed new light on the relative contribution of the changes in solubility and the processes related to changes in AOU to the observed variability of the oxygen concentration in the LSW layer. We found that the variations in  $\text{O}_2^{\text{sat}}$  account only for 17% of the total oxygen variability over the 28-years period, while most of it was related with changes in AOU (73%). However, the relative contribution of both terms, as well as the processes explaining the changes in AOU, vary over interannual to decadal scales depending on the dynamical features in the Irminger Sea. During the periods of intense convection in the 90's ( $P_1$ ), when the subpolar gyre was cold and the mixed layer was deep, the oxygen concentration is close to 93% of  $\text{O}_2^{\text{sat}}$ . This percentage has been reported as the average value of the maximum oxygen saturation that can be reached in the mixed layer under deep convection episodes in the Labrador Sea<sup>12,13,15</sup>. Thus, the smaller AOU estimated during this period can be attributed to strong ventilation and oxygen uptake.

During the 2002–2014 period, when  $\text{O}_2^{\text{sat}}$  was lower, convection was generally weak, and the observed undersaturation cannot be mainly attributed to vertical mixing<sup>13</sup>. Thus, the higher AOU within the LSW layer likely resulted from a combination between (little) vertical mixing, biological consumption, and, mainly, changes in lateral advection that may have increased the water age. Nevertheless, during this period, the AOU exhibits important interannual variability. Peaks of low AOU coincide with high oxygen concentration that can be explained by larger deep convection events that took place during the warm phase of the subpolar gyre<sup>11,15,18</sup>.

In contrast, during the  $P_3$  period (2015–2018), AOU progressively diminishes, and the observed oxygen concentration only approaches 93% of  $\text{O}_2^{\text{sat}}$  in 2017–2018. The relatively high values of AOU during the deepest convection years (2015 and 2016) could be attributed to the continuous entrainment of

undersaturated waters from the less oxygenated and deeper LSW as the mixed layer deepens until its deepest level in 2016. After 2016, the convection gets shallower, so the entrained waters that have been ventilated the previous winter are more oxygenated, and the mixed layer waters re-saturate quicker<sup>13</sup>. Thus, AOU progressively decreases, and the oxygen concentration approaches again the 93% of  $O_2^{\text{sat}}$ .

To the best of our knowledge, our results allowed us, for the first time, to attribute the observed change in oxygen concentration of the LSW layer in the Irminger Sea to different processes that took place in the North Atlantic. These processes are tied to the natural interannual-to-multidecadal variability of the subpolar gyre that has been reported in previous studies. Indeed, the atmospheric forcing and the oxygen content are connected in different ways: (i) positive NAO index implies increased heat loss, stronger winds, stronger WSC, and enhanced winter convection in the Irminger Sea<sup>18</sup>, (ii) stronger WSC contributes to an intensification of the subpolar gyre, and (iii) the previous points (i) and (ii) are associated with less stratified and cooler surface waters<sup>23</sup>. Under these conditions, from 2015 and during successive winters until 2018, strong convection events associated with cold and deep mixed layers explained the deeper ventilation, a progressive reduction in the water age (AOU), thus an increase of the oxygen concentration in the LSW.

During the 90s, winter MLD data are not available, but the intensity of the NAO and the WSC, as well as the thick and deep characteristics of the LSW, are similar to those between 2015 and 2018. Therefore, we hypothesize that similar processes are responsible for the high oxygen concentration of the LSW in both periods. In between, negative NAO and WSC have favored weaker, warmer and more stratified gyre, thus shallower ventilation and lower oxygen concentration.

During the beginning and the end of the time series ( $P_1$  and  $P_3$ ), part of the newly ventilated LSW formed in the Labrador Sea could be advected into the Irminger Sea, partly contributing to its high oxygen concentration. However, during deep convection events, the remote LSW is likely re-ventilated and re-saturated, which complicates the quantitative assessment of the role of advection in the observed oxygen variability in the Irminger sea. More resolved current data or model study would be necessary to separate the local and advected LSW and understand the effects on oxygen variability. In this context, one blind spot of our study is the role of biological consumption in the ventilated region. The role of biological activity on the North Atlantic subpolar gyre is complex and not fully understood, especially during winter<sup>27</sup>. In this highly dynamic region, where the physical drivers of the ventilation are dominant, we have not disentangled the contribution of biological consumption that modulates the AOU over the studied period. This question could be addressed with sustained observation of full BGC parameters in the context of Biogeochemical Argo mission<sup>28</sup>. Although this study demonstrates the value of combining the sustained Argo and hydrological oxygen sampling in the North Atlantic, longer OneArgo sampling, especially for full BGC parameters, combined with improved model studies could help address those questions. Last, it would be interesting to study the oxygen variability in the deeper water masses, i.e., in the Iceland Scotland Overflow Water (ISOW) and Denmark Strait Overflow Water (DSOW), and in relation with the LSW oxygen variability. Note that Argo profiles only reach 2000 m depth and, therefore, do not resolve the full water column, notably the ISOW (classically defined between the 27.8 and 27.85  $\text{kg m}^{-3}$  and found below 2000 m<sup>29</sup>), and the DSOW (potential density higher than 27.88  $\text{kg m}^{-3}$ <sup>30</sup>). Therefore, more deep Argo floats with oxygen sensor would be necessary to fully resolve the ISOW and DSOW layers.

Over the time period 1991–2018, we did not observe any significant linear trend of the oxygen content either within the LSW, or over the entire water column. The natural oxygen variability in the LSW linked to that of the subpolar gyre, together with the relative short record that we have available (28 years) makes it difficult to determine whether anthropogenic-induced changes in the oxygenation of the LSW have occurred<sup>31</sup>. The North Atlantic is one of the regions of the world where no significant warming<sup>32–34</sup> or deoxygenation trends<sup>1,4</sup> are observed, and it is rather dominated by the natural decadal variability. However, in a warming ocean, the surface heating, glacier melt, and increased precipitation at high latitudes will likely increase the ocean stratification<sup>4,35,36</sup>. This is thought to lead to a reduced ventilation of the interior ocean and the AMOC strength<sup>37</sup>. In the North Atlantic Ocean, the role of these long-term players on the ocean oxygen ventilation are still to be elucidated.

## Methods

**Argo data and products.** The data from the observational Argo array<sup>38,39</sup> were downloaded from the ftp server of the French Global Data Assembly Center Coriolis<sup>40</sup>. We selected the profiles containing oxygen, temperature, and practical salinity data available in delayed mode and we used only those with Quality Control (QC) flag set to 1 and 2 (i.e., 'good' and 'probably good' data, see reference Table 2 in the Argo report<sup>41</sup>). Argo floats typically sample down to 2000 m. We have then extracted the profiles located in the core of the Irminger Sea region, which was defined by the area within the bathymetric contour of 2700 m (Fig. 1). Within the core of the Irminger Sea, a collection of 581 profiles from 27 Argo floats was obtained between 2010 and 2018. All the properties, i.e., potential temperature ( $\theta$ ), practical salinity, dissolved oxygen, and potential density anomaly ( $\sigma_\theta$ ) were monthly averaged within this area. We ensured that neither temporal and spatial biases were found in the yearly nor in the monthly distribution of the profiles (Figs. S1 and S2). The spatial variability of the LSW oxygen concentration within this Irminger Sea region is accounted for in our computations of the uncertainty of the Irminger basin averages of hydrological and oxygen parameters.

In addition, we used two Argo-based products: the ANDRO product<sup>42</sup> and the In Situ Analysis System (ISAS) product<sup>43</sup>. ANDRO is a quality-controlled subsurface displacement dataset for the global ocean from all Argo floats from January 2010 (with more than 1.2 million deep displacements). Every cycle, the Argo floats dive to the parking depth, typically 1000 m, where they drift during about 9-days before descending to 2000 m and then rising to the sea surface while performing all the measurements. The deep displacement of Argo floats at this parking depth is used to map the ocean circulation at 1000 m depth and its variability. We then computed the relative vorticity from the meridional and zonal velocity ( $\zeta = \frac{dv}{dx} - \frac{du}{dy}$ ), and averaged it over consecutive and overlapping 4-year periods. Last, the anomaly of the relative vorticity is computed by removing the mean value.

ISAS is a 3D gridded product derived from monthly optimal interpolation of temperature and salinity data from 2002 to 2020<sup>43</sup>. ISAS was used to compute the mixed layer depth (MLD) and temperature (MLT) between 2010 and 2018 as well as for obtaining the mean oxygen concentration at 1000 m shown in Fig. 1.

MLD was computed by using a criterion based on a density difference between the surface and the base of the mixed layer<sup>44</sup> of  $\Delta\sigma_\theta = 0.03 \text{ kg m}^{-3}$ . The criteria to compute the MLD on individual in situ profiles in the North Atlantic subpolar gyre<sup>15</sup> is usually  $\Delta\sigma_\theta = 0.01 \text{ kg m}^{-3}$ . However, ISAS is a gridded product that tends to smooth the profiles. Thus, using ISAS with a smaller density criterion may underestimate the depth of the mixed layer. MLT was averaged over the winter each year (January to March). Then winter MLT and MLD were spatially averaged in the defined area within the core of the Irminger Sea (Fig. 1).

**Hydrographic sections.** Along with Argo data, we obtained potential temperature, practical salinity and dissolved oxygen data from 15 ship-based hydrographic sections in the Irminger Sea: nine OVIDE (Observatoire de la variabilité interannuelle et décennale en Atlantique Nord<sup>45</sup>) sections that were performed every two years from 2002 to 2018, four AR07E (Atlantic Repeat Hydrography Line 7 East) sections (two in 1991, one in 1992, and one in 1997), and two A01E (Atlantic Repeat Hydrography Line 1) sections (1991 and 1994). These cruises were conducted at approximately the same time of the year (from June to September, except for two: the AR07E section in 1991 which was conducted in April, and the A01E section in 1994, in November). All the OVIDE, AR07E, and A01E cruises were performed along the same section between 45° W and 30° W in the Irminger Sea (Fig. 1). We thus interpolated all these sections along a regular longitudinal axis. For the OVIDE data, the accuracy of the temperature, salinity, pressure and oxygen measurements<sup>46,47</sup> are better than 0.002 °C, 0.002, 1 dbar and 3  $\mu\text{mol kg}^{-1}$ , respectively.

The combined use of the hydrographic cruises and Argo data allowed us to extend the Argo time series back in time and in depth until 3000 m, and it



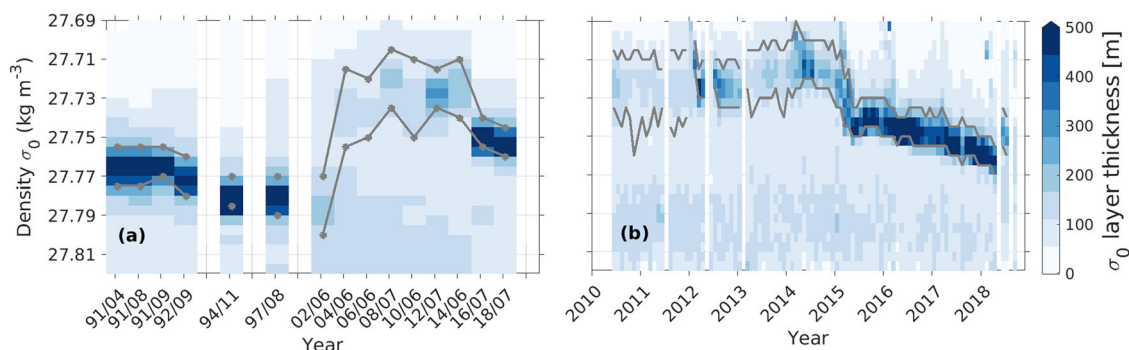


**Fig. 6 Labrador Sea water thickness.** Time series of the density layer thickness for  $\sigma_0$  intervals of  $0.005 \text{ kg m}^{-3}$  averaged within the core of the Irminger Sea (Fig. 1), **a** for the hydrographic profiles and **b** for the Argo data. Gray curves and points highlight the lower and upper boundaries of the Labrador Sea Water layer (LSW). Note that the x-axis is not evenly spaced in **a**, and that the longest gaps are marked with a blank space. In **b**, the vertical white lines indicate missing data for interpolation.

reinforces the robustness of our results. Furthermore, thanks to high temporal resolution of Argo data, we have corroborated that the oxygen concentration along the hydrographic sections is representative of the decadal variability of oxygen concentration and was not biased by the seasonal cycle (cruises take place generally during summer) or interannual events within the Irminger Sea region. When averaging the Argo oxygen profiles within the Irminger Sea and over the period when the hydrographic sections are performed, the data agree within  $5 \mu\text{mol kg}^{-1}$ , which lays within the hydrographic and Argo data uncertainties<sup>48</sup>. All available profiles were interpolated onto a regular depth axis going from the surface down to 2000 m for the Argo data and down to 3000 m for the hydrographic data, with a 5 m resolution.

**Wind data and NAO index.** Wind speed and wind-stress were obtained from the NCEP reanalysis<sup>49</sup>. The fields were available every 6 h from 1990 to 2018 at a horizontal resolution of  $2^\circ$  in longitude and latitude. The Wind Stress Curl (WSC) was computed using the meridional and zonal wind stress component and 6-hourly outputs of the surface wind stress have been used for the computation ( $\text{WSC} = \frac{d\tau_y}{dx} - \frac{d\tau_x}{dy}$  in  $\text{N m}^{-3}$ ). In addition, we obtained the NAO index from the UCAR Climate Data Guide website<sup>50</sup>. The NAO index is based on the surface sea-level pressure difference between the Subtropical High (Azores) and the Subpolar Low (Iceland). The NAO is the dominant mode of atmospheric variability in the North Atlantic ocean, a positive NAO index is expected to favor the occurrence of deep convection in the North Atlantic subpolar gyre because of stronger wind and colder waters than during negative phase of NAO<sup>26</sup>. Data were available from 1990 to 2018. The winter WSC anomalies were computed relative to the mean value of the 1990–2018 period and averaging the values from January to March. The winter anomalies of the NAO were computed by removing its seasonal cycle and then averaging the values from January to March.

**Sea level anomalies.** To estimate the strength of the subpolar gyre and in addition to the ANDRO dataset that provided the velocity field at 1000 m depth, we used the detrended annual-mean sea-level anomaly (SLA) within the subpolar gyre obtained from Satellite Altimetry (Aviso multi-sensor altimetry data<sup>23</sup>).

**Oxygen solubility and AOU computation.** To get more insight on the processes behind the oxygen variability, we computed the oxygen concentration at 100% saturation ( $\text{O}_2^{\text{sat}}$ ) and the Apparent Oxygen Utilization ( $\text{AOU} = \text{O}_2^{\text{sat}} - \text{O}_2$ ).  $\text{O}_2^{\text{sat}}$  represents the oxygen concentration that a water mass with given temperature and salinity can reach when in equilibrium with the atmosphere. It is computed following Weiss (1970)'s formulation of oxygen solubility and depends mainly on temperature and only slightly on salinity. Previous studies have estimated the oxygen undersaturation in the mixed layer during deep convection periods in the North Atlantic (Irminger and Labrador seas) to vary between 3% and 10%, with an average estimated value of around 7%<sup>12,13,15,16</sup>. Therefore, to help in the interpretation of the drivers of oxygen variability we have computed the 93% of  $\text{O}_2^{\text{sat}}$  for comparative purposes (Fig. 2).

AOU can be considered as a proxy of the water-mass age and it represents the combined effect of oxygen consumption from the remineralization of organic matter, and vertical and horizontal mixing between waters with different oxygen concentration<sup>6</sup>. High AOU values are usually found in waters with remote origin that have undergone mixing with lower oxygenated water and/or biological consumption along their path to the sampling location. Low AOU values are found in waters that are newly ventilated without much mixing or biological history. Therefore, AOU can provide complementary information on the role of the circulation and its changes on the oxygen content that cannot be revealed from measurements of physical properties, such as temperature and salinity<sup>51</sup>.

**Definition of the LSW.** The LSW plays a key role for climate by transferring surface water properties and tracers of atmospheric origin into the ocean interior. Therefore, the LSW layer is the focus of this study. It is formed by intense winter buoyancy loss and mixing during winter convection either locally in the Irminger Sea, or in the Labrador Sea from where it is advected<sup>15,17</sup>. The LSW is characterized by a weakly stratified core (low potential vorticity<sup>52</sup>) and high oxygen concentration. It also exhibits a minimum in salinity within the water column.

The LSW is usually defined as the water mass laying between the 27.7 and  $27.8 \text{ kg m}^{-3}$  isopycnals<sup>17,53</sup>. However, it has been shown that the LSW density varies over time<sup>10,31</sup> and, therefore, its definition by fixed isopycnals can be misleading. We performed a density layer analysis within the Irminger Sea to define the LSW layer accurately (Fig. 6), and based on previous studies<sup>10,31,54</sup>. The reader is referred to the aforementioned studies for more details about the methods used to define the LSW layer. In particular in our study, we computed the thickness of potential density  $\sigma_0$  layers from top to bottom, and the LSW layer was defined within the densities that fall within the 73% of the maximum  $\sigma_0$  layer. The maximum isopycnal layer thickness of LSW over the sampling period ranged between 380 and 500 m (Fig. 3).

## Data availability

Argo data were collected and made freely available by the International Argo Program and the national programs that contribute to it (<http://www.argo.ucsd.edu>, <http://argo.jcommops.org>). The Argo Program is part of the Global Ocean Observing System. The NAO data were downloaded from the UCAR Climate Data Guide website<sup>50</sup>: <https://climatedataguide.ucar.edu/climate-data/hurrell-north-atlantic-oscillation-nao-index-pc-based>. OVIDE, AR07E and AO1 data are available from the CLIVAR Carbon Hydrographic Data Office (CCHDO, <https://cchdo.ucsd.edu/>). NCEP data were downloaded from the Research Data Archive at NOAA/PSL: <https://rda.ucar.edu/datasets/ds082/>. ANDRO argo floats displacements product is made freely available by SNO Argo France at LOPS Laboratory (supported by UBO/CNRS/Ifremer/IRD) and IUEM Observatory (OSU IUEM/CNRS/INSU), and was funded by Ifremer, Coriolis, SOERE-CTD02 and SNO Argo France at <https://doi.org/10.17882/47077>. ISAS temperature and salinity monthly gridded field products are made freely available by SNO Argo France at LOPS Laboratory (supported by UBO/CNRS/Ifremer/IRD) and IUEM Observatory (OSU IUEM/CNRS/INSU) at <https://doi.org/10.17882/52367>. The altimeter products were produced by Ssalto/Duacs and distributed by Aviso, with support from CNES (<http://www.aviso.altimetry.fr/duacs/>).

Received: 14 January 2022; Accepted: 29 September 2022;

Published online: 12 November 2022

## References

- Schmidt, S., Stramma, L. & Visbeck, M. Decline in global oceanic oxygen content during the past five decades. *Nature* **542**, 335–339 (2017).
- Bopp, L., Le Quéré, C., Heimann, M., Manning, A. C. & Monfray, P. Climate-induced oceanic oxygen fluxes: Implications for the contemporary carbon budget. *Glob. Biogeochem. Cycles* **16**, 6–1613 (2002).
- IPCC: IPCC, 2021: Climate Change 2021: The Physical Science Basis. Contribution of Working Group I to the Sixth Assessment Report of the Intergovernmental Panel on Climate Change. (Cambridge University Press, 2021).



4. Helm, K. P., Bindoff, N. L. & Church, J. A. Observed decreases in oxygen content of the global ocean. *Geophys. Res. Lett.* **38** <https://doi.org/10.1029/2011GL049513> (2011).
5. Li, G. et al. Increasing ocean stratification over the past half-century. *Nat. Clim. Change* **10**, 1116–1123 (2020).
6. Stendardo, I. & Gruber, N. Oxygen trends over five decades in the north atlantic. *J. Geophys. Res.: Oceans* **117** <https://doi.org/10.1029/2012JC007909> (2012).
7. Couespel, D., Lévy, M. & Bopp, L. Major contribution of reduced upper ocean oxygen mixing to global ocean deoxygenation in an earth system model. *Geophys. Res. Lett.* **46**, 12239–12249 (2019).
8. Portela, E., Kolodziejczyk, N., Vic, C. & Thierry, V. Physical mechanisms driving oxygen subduction in the global ocean. *Geophys. Res. Lett.* **47**, 2020–089040 (2020).
9. Dickson, R., Lazier, J., Meincke, J., Rhines, P. & Swift, J. Long-term coordinated changes in the convective activity of the North Atlantic. *Progr. Oceanogr.* **38**, 241–295 (1996).
10. Yashayaev, I. & Loder, J. W. Recurrent replenishment of Labrador Sea Water and associated decadal-scale variability. *J. Geophys. Res.: Oceans* **121**, 8095–8114 (2016).
11. Fröb, F. et al. Irminger sea deep convection injects oxygen and anthropogenic carbon to the ocean interior. *Nat. Commun.* **7**, 13244 (2016).
12. Clarke, R. A. & Coote, A. R. The formation of labrador sea water. part iii: The evolution of oxygen and nutrient concentration. *J. Phys. Oceanogr.* **18**, 469–480 (1988).
13. Wolf, M. K., Hamme, R. C., Gilbert, D., Yashayaev, I. & Thierry, V. Oxygen saturation surrounding deep water formation events in the labrador sea from argo-o2 data. *Glob. Biogeochem. Cycles* **32**, 635–653 (2018).
14. Dickson, R. & Brown, J. The production of north atlantic deep water: sources, rates, and pathways. *J. Geophys. Res.: Oceans* **99**, 12319–12341 (1994).
15. Piron, A., Thierry, V., Mercier, H. & Caniaux, G. Argo float observations of basin-scale deep convection in the Irminger sea during winter 2011–2012. *Deep Sea Res. Part I: Oceanogr. Res. Papers* **109**, 76–90 (2016).
16. Koelling, J., Wallace, D. W. R., Send, U. & Karstensen, J. Intense oceanic uptake of oxygen during 2014–2015 winter convection in the labrador sea. *Geophys. Res. Lett.* **44**, 7855–7864 (2017).
17. Kieke, D. et al. Changes in the CFC inventories and formation rates of Upper Labrador Sea Water, 1997–2001. *J. Phys. Oceanogr.* **36**, 64–86 (2006).
18. Piron, A., Thierry, V., Mercier, H. & Caniaux, G. Gyre-scale deep convection in the subpolar north atlantic ocean during winter 2014–2015. *Geophys. Res. Lett.* **44**, 1439–1447 (2017).
19. Pickart, R. S. et al. Is Labrador Sea Water formed in the Irminger basin? *Deep Sea Res. Part I: Oceanogr. Res. Papers* **50**, 23–52 (2003).
20. Körtzinger, A., Schimanski, J., Send, U. & Wallace, D. The ocean takes a deep breath. *Science* **306**, 1337–1337 (2004).
21. de Jong, M. F., van Aken, H. M., Våge, K. & Pickart, R. S. Convective mixing in the central irmingier sea: 2002–2010. *Deep Sea Res. Part I: Oceanogr. Res. Papers* **63**, 36–51 (2012).
22. de Jong, M. F., Oltmanns, M., Karstensen, J. & de Steur, L. Deep convection in the irmingier sea observed with a dense mooring array. *Oceanography* **31**, 50–59 (2018).
23. Chafik, L., Nilsen, J. E. Ø., Dangendorf, S., Reverdin, G. & Frederikse, T. North atlantic ocean circulation and decadal sea level change during the altimetry era. *Sci. Rep.* **9**, 1041 (2019).
24. Marshall, J. & Schott, F. Open-ocean convection: Observations, theory, and models. *Rev. Geophys.* **37**, 1–64 (1999).
25. Våge, K. et al. Surprising return of deep convection to the subpolar north atlantic ocean in winter 2007–2008. *Nat. Geosci.* **2**, 67–72 (2009).
26. Hurrell, J. W. Decadal trends in the North Atlantic oscillation: regional temperatures and precipitation. *J. Mar. Syst.* **269**, 676–679 (1995).
27. Behrenfeld, M. J. Abandoning sverdrup's critical depth hypothesis on phytoplankton blooms. *Ecology* **91**, 977–989 (2010).
28. Mignot, A., Ferrari, R. & Claustre, H. Floats with bio-optical sensors reveal what processes trigger the north atlantic bloom. *Nat. Commun.* **9**, 190 (2018).
29. García-Ibáñez, M. I. et al. Water mass distributions and transports for the 2014 geovide cruise in the north atlantic. *Biogeosciences* **15**, 2075–2090 (2018).
30. Tanhua, T., Olsson, K. A. & Jeansson, E. Formation of denmark strait overflow water and its hydro-chemical composition. *J. Mar. Syst.* **57**, 264–288 (2005).
31. Yashayaev, I. & Loder, J. W. Further intensification of deep convection in the labrador sea in 2016. *Geophys. Res. Lett.* **44**, 1429–1438 (2017).
32. Häkkinen, S., Rhines, P. B. & Worthen, D. L. Heat content variability in the north atlantic ocean in ocean reanalyses. *Geophys. Res. Lett.* **42**, 2901–2909 (2015).
33. Häkkinen, S., Rhines, P. B. & Worthen, D. L. Warming of the global ocean: spatial structure and water-mass trends. *J. Clim.* **29**, 4949–4963 (2016).
34. Johnson, G. C. & Lyman, J. M. Warming trends increasingly dominate global ocean. *Nat. Clim. Change* **10**, 757–761 (2020).
35. Gruber, N. Warming up, turning sour, losing breath: ocean biogeochemistry under global change. *Philos. Trans. R. Soc. A: Math., Phys. Eng. Sci.* **369**, 1980–1996 (2011).
36. Böning, C. W., Behrens, E., Biastoch, A., Getzlaff, K. & Bamber, J. L. Emerging impact of greenland meltwater on deepwater formation in the north atlantic ocean. *Nat. Geosci.* **9**, 523–527 (2016).
37. Lique, C. & Thomas, M. D. Latitudinal shift of the atlantic meridional overturning circulation source regions under a warming climate. *Nat. Clim. Change* **8**, 1013–1020 (2018).
38. Roemmich, D. et al. On the future of argo: a global, full-depth, multi-disciplinary array. *Front. Mar. Sci.* **6**, 439 (2019).
39. Wong, A. P. S. et al. Argo data 1999–2019: Two million temperature-salinity profiles and subsurface velocity observations from a global array of profiling floats. *Front. Mar. Sci.* **7**, 700 (2020).
40. Argo: Argo float data and metadata from Global Data Assembly Centre (Argo GDAC). <https://doi.org/10.17882/42182> (2021).
41. Argo: Argo user's manual v3.41. Report. <https://doi.org/10.13155/29825> (2021).
42. Ollitrault, M. & Rannou, J.-P. Andro: an argo-based deep displacement dataset. *J. Atmos. Ocean. Technol.* **30**, 759–788 (2013).
43. Gaillard, F., Reynaud, T., Thierry, V., Kolodziejczyk, N. & von Schuckmann, K. In situ-based reanalysis of the global ocean temperature and salinity with isas: variability of the heat content and steric height. *J. Clim.* **29**, 1305–1323 (2016).
44. De Boyer Montégut, C., Madec, G., Fischer, A. S., Lazar, A. & Iudicone, D. Mixed layer depth over the global ocean: an examination of profile data and a profile-based climatology. *J. Geophys. Res.: Oceans* **109**, 12003 (2004).
45. OVIDE: Ovide group. The ovide set of cruises. french oceanographic cruises directory. <https://doi.org/10.18142/140> (2021).
46. Branellec, P. & Thierry, V. Ovide 2010 ctd-o2 cruise report. Report (scientific report). <https://archimer.ifremer.fr/doc/00210/32134/> (2013).
47. Daniault, N. et al. The northern north atlantic ocean mean circulation in the early 21st century. *Prog. Oceanogr.* **146**, 142–158 (2016).
48. Thierry, V. & Bittig, H. Argo quality control manual for dissolved oxygen concentration. Report (qualification paper (procedure, accreditation support)). <https://doi.org/10.13155/46542> (2021).
49. Kalnay, E. et al. The ncep/ncar 40-year reanalysis project. *Bull. Am. Meteorol. Soc.* **77**, 437–472 (1996).
50. Schneider, D. P., Deser, C., Fasullo, J. & Trenberth, K. E. Climate data guide spurs discovery and understanding. *Eos, Trans. Am. Geophys. Union* **94**, 121–122 (2013).
51. Keeling, R. F., Körtzinger, A. & Gruber, N. Ocean deoxygenation in a warming world. *Annu. Rev. Mar. Science* **2**, 199–229 (2009).
52. Talley, L. D. & McCartney, M. S. Distribution and circulation of labrador sea water. *J. Phys. Oceanogr.* **12**, 1189–1205 (1982).
53. Stramma, L. et al. Deep water changes at the western boundary of the subpolar North Atlantic during 1996 to 2001. *Deep Sea Res. Part I: Oceanogr. Res. Papers* **51**, 1033–1056 (2004).
54. Feucher, C., Garcia-Quintana, Y., Yashayaev, I., Hu, X. & Myers, P. G. Labrador sea water formation rate and its impact on the local meridional overturning circulation. *J. Geophys. Res.: Oceans* **124**, 5654–5670 (2019).

## Acknowledgements

C.F. was supported by SAD postdoctoral program of French Brittany Region and co-funded by Ifremer. This research has been supported by the French government within the framework of the "Investissements d'avenir" program managed by the Agence Nationale de la Recherche under the NAOS project (grant no. ANR-10-EQPX-40) and ARGO-2030 project (grant no. ANR-21-ESRE-0019). This work is a contribution to the OVIDE project supported by CNRS, Ifremer, the national program LEFE (Les Enveloppes Fluides et l'Environnement) and the Spanish Ministry of Sciences and Innovation co-funded by the BOCATS2 project (grant no. PID2019-104279GB-C21) and ARIOS project (grant no. CTM2016-76146-C3-1-R). We are also grateful to three anonymous reviewers for their constructive and insightful comments, which help us to improve our manuscript.

## Author contributions

The idea of this study was conceived by C.F., E.P., N.K., and V.T. C.F. conducted most of the data analysis and created the figures. The manuscript was written by C.F. with valuable input from all authors. Proposal for project funding was written by E.P., N.K., and V.T.

## Competing interests

The authors declare no competing interests.

## Additional information

**Supplementary information** The online version contains supplementary material available at <https://doi.org/10.1038/s43247-022-00570-y>.

**Correspondence** and requests for materials should be addressed to Charlène Feucher.

**Peer review information** *Communications Earth & Environment* thanks the anonymous reviewers for their contribution to the peer review of this work. Primary Handling Editors: Viviane V. Menezes and Clare Davis.

**Reprints and permission information** is available at <http://www.nature.com/reprints>

**Publisher's note** Springer Nature remains neutral with regard to jurisdictional claims in published maps and institutional affiliations.



**Open Access** This article is licensed under a Creative Commons Attribution 4.0 International License, which permits use, sharing, adaptation, distribution and reproduction in any medium or format, as long as you give appropriate credit to the original author(s) and the source, provide a link to the Creative Commons license, and indicate if changes were made. The images or other third party material in this article are included in the article's Creative Commons license, unless indicated otherwise in a credit line to the material. If material is not included in the article's Creative Commons license and your intended use is not permitted by statutory regulation or exceeds the permitted use, you will need to obtain permission directly from the copyright holder. To view a copy of this license, visit <http://creativecommons.org/licenses/by/4.0/>.

© The Author(s) 2022